

Transcriptional profile and chromatin accessibility in zebrafish melanocytes and melanoma tumors

Eva T. Kramer, Paula M. Godoy, and Charles K. Kaufman*

Division of Medical Oncology, Departments of Medicine and Developmental Biology, Washington University in Saint Louis, St Louis, MO 63110, USA

*Corresponding author: Division of Medical Oncology, Departments of Medicine and Developmental Biology, Washington University School of Medicine, 4518 McKinley Avenue, St Louis, MO 63110, USA. Email: ckkaufman@wustl.edu

Abstract

Transcriptional and epigenetic characterization of melanocytes and melanoma cells isolated from their *in vivo* context promises to unveil key differences between these developmentally related normal and cancer cell populations. We therefore engineered an enhanced *Danio rerio* (zebrafish) melanoma model with fluorescently labeled melanocytes to allow for isolation of normal (wild type) and premalignant ($BRAF^{V600E}$ -mutant) populations for comparison to fully transformed $BRAF^{V600E}$ -mutant, *p53* loss-of-function melanoma cells. Using fluorescence-activated cell sorting to isolate these populations, we performed high-quality RNA- and ATAC-seq on sorted zebrafish melanocytes vs. melanoma cells, which we provide as a resource here. Melanocytes had consistent transcriptional and accessibility profiles, as did melanoma cells. Comparing melanocytes and melanoma, we note 4128 differentially expressed genes and 56,936 differentially accessible regions with overall gene expression profiles analogous to human melanocytes and the pigmentation melanoma subtype. Combining the RNA- and ATAC-seq data surprisingly revealed that increased chromatin accessibility did not always correspond with increased gene expression, suggesting that though there is widespread dysregulation in chromatin accessibility in melanoma, there is a potentially more refined gene expression program driving cancerous melanoma. These data serve as a resource to identify candidate regulators of the normal vs. diseased states in a genetically controlled *in vivo* context.

Keywords: zebrafish; melanocytes; melanoma; RNA-seq; ATAC-seq

Introduction

Human melanoma is notable as one of the most highly mutagenized cancers, making comparisons between patient samples difficult given variation in potentially irrelevant passenger somatic mutations in addition to the background of an outbred heterogeneous population (Hodis *et al.* 2012). Genetically engineered tumor models allow for comparisons of premalignant and cancer cells between highly related individuals (*e.g.*, siblings, cousins) with defined driver and tumor suppressor mutations. A zebrafish model combining a $BRAF^{V600E}$ mutation, present in over 50% of human melanomas, with a loss of function (*lf*) in *p53* develops one to three melanomas in its lifetime (Patton *et al.* 2005). Despite high genetic relatedness, the $Tg(BRAF^{V600E})/p53^{lf/lf}$ tumors still display genomic heterogeneity but without clear functional consequences in this model (Yen *et al.* 2013). High heterogeneity in melanoma can lead to variable responses to currently available therapies (Reuben *et al.* 2017). To continue to identify novel melanoma therapies, we must delve deeper into the transcriptional and epigenetic differences that exist between the normal and diseased states.

Many studies have utilized next-generation sequencing technologies to evaluate melanoma subtypes based on clinicopathological characteristics (Cancer Genome Atlas Network 2015; Hayward *et al.* 2017; Tsoi *et al.* 2018; Rabbie *et al.* 2019; Cisarova

et al. 2020; Durante *et al.* 2020), major mutations (Cancer Genome Atlas Network 2015; Travnickova *et al.* 2019), and drug resistance and survival (Rambow *et al.* 2018; Garg *et al.* 2021). Prior studies comparing melanocytes and cutaneous melanoma cells have reported on coding mutations, gene expression changes only, or have used human or zebrafish cell lines rather than focusing on *in vivo* animal models (Yen *et al.* 2013; Haltaufderhyde and Oancea 2014; Kaufman *et al.* 2016; Badal *et al.* 2017; Kunz *et al.* 2018; Venkatesan *et al.* 2018; Marie *et al.* 2020; Wouters *et al.* 2020). Single-cell RNA-seq experiments so far generally focus on the heterogeneity within cell populations, rather than a comparison between melanocytes and melanoma cells, or they do not evaluate the epigenetic landscape (Ennen *et al.* 2015; Tirosh *et al.* 2016; Gan *et al.* 2018; Rambow *et al.* 2018; Baron *et al.* 2020; Li *et al.* 2020; Belote *et al.* 2021; Travnickova and Patton 2021). Thus, we sought to characterize the epigenetic and transcriptional differences between zebrafish nonmalignant, precancerous, and malignant melanocytes in a genetically defined melanoma context.

Since its initial report in 2013, Assay for Transposase Accessible Chromatin with high-throughput sequencing (ATAC-seq) has become a widely used method to provide a sensitive assessment of genomic accessibility (Buenrostro *et al.* 2013). The combination of epigenetic and transcriptional approaches has been used to decipher regulators in hematopoiesis and leukemia

Received: June 22, 2021. Accepted: October 02, 2021

© The Author(s) 2021. Published by Oxford University Press on behalf of Genetics Society of America.

This is an Open Access article distributed under the terms of the Creative Commons Attribution License (<https://creativecommons.org/licenses/by/4.0/>), which permits unrestricted reuse, distribution, and reproduction in any medium, provided the original work is properly cited.

(Corces et al. 2016), find loci influencing pancreatic α - and β -cell differentiation (Ackermann et al. 2016), identify regions influencing gestational duration (Sakabe et al. 2020), characterize intermediate states in melanoma cell cultures (Wouters et al. 2020), among many other applications. Still, a comparison of the epigenetic and transcriptional profiles of sorted normal melanocytes to melanoma tumors in a native, *in vivo* biological context utilizing an animal model has been limited, thus diminishing our ability to dissect mechanisms governing melanoma initiation.

Animal models represent a powerful tool to understand disease initiation and progression, discover therapeutic targets, and test drugs. Utilizing the Tg(BRAF^{V600E})/p53^{lf/lf} zebrafish model, we probed the natural biological context of normal melanocytes and related disease development, specifically that of melanoma cancer, using RNA- and ATAC-seq (Patton et al. 2005; White et al. 2011; Kaufman et al. 2016). Furthermore, we compared the transcriptional profiles of zebrafish melanocytes (MC) and melanoma cells (MA) to existing human RNA-seq datasets classifying subtypes of melanoma (Jönsson et al. 2010; Harbst et al. 2012; Cancer Genome Atlas Network 2015; Cirenajwis et al. 2015; Nsengimana et al. 2015; Lauss et al. 2016; Badal et al. 2017; Gan et al. 2018; Kunz et al. 2018) to further confirm the relevance of these animal models. We present a transcriptomic and genome-wide chromatin accessibility analysis of precancerous MC and fully transformed MA in the most widely used zebrafish melanoma model to be used as a resource for identifying pathways, genes, and loci which differentiate melanoma from normal pigment cells.

Materials and methods

Zebrafish husbandry

Zebrafish were raised in the Washington University Zebrafish Consortium in accordance with animal protocols and the Washington University IACUC. Pair or harem crosses generated embryos, which were then raised at 28.5°C. The following wild type (WT), mutant, and transgenic strains were utilized: AB*, Tg(MiniCoopR; mitfa:mCherry), Tg(mitfa:BRAF^{V600E}); p53^{lf/lf}, Tg(crestin:EGFP), Tg(mitfa:BRAF^{V600E/+}); p53^{+/lf}; mitfa^{+/-}; Tg(MiniCoopR; mitfa:mCherry), Tg(mitfa:BRAF^{V600E})/p53^{lf/lf}/mitfa^{+/-}/Tg(MiniCoopR; mitfa:mCherry) and Tg(mitfa:BRAF^{V600E}); p53^{lf/lf}; mitfa^{-/-}.

Transgenic fish generation

First, we injected WT AB* zebrafish with MiniCoopR:mitfa:mCherry. Fish with germline transmission of Tg(MiniCoopR; mitfa:mCherry) (source of MC_{WT}) were then crossed to Tg(mitfa:BRAF^{V600E}); p53^{lf/lf}; mitfa^{-/-} zebrafish and scored for presence of mCh+ melanocytes. These Tg(mitfa:BRAF^{V600E/+}); p53^{+/lf}; mitfa^{+/-}; mitfa:mCherry fish (source of MC_{Het}) were crossed to Tg(mitfa:BRAF^{V600E}); p53^{lf/lf}; mitfa^{-/-} zebrafish and scored for presence of mCh+ melanocytes, and PCR genotyped for BRAF and p53 status to confirm generation of Tg(mitfa:BRAF^{V600E})/p53^{lf/lf}/mitfa^{+/-}/mitfa:mCherry zebrafish (source of MC_{Homo}).

Tissue collection

For RNA-seq, we utilized mCh+ melanocytes sorted from the skin of three independent AB* zebrafish expressing MiniCoopR:mitfa:mCherry, three independent zebrafish heterozygous for Tg(BRAF^{V600E/+})/p53^{+/lf}/mitfa^{+/-}, and GFP+ melanoma tumor cells from five distinct tumors from three Tg(BRAF^{V600E})/p53^{lf/lf}/Tg(crestin:EGFP) fish. The melanoma samples from MA3A, MA3B, and MA3C were isolated from one fish with three tumors: a tumor near the dorsal fin, a tumor on the tail, and a tumor on the head. For ATAC-seq, we utilized mCh+ melanocytes from three zebrafish

heterozygous for Tg(BRAF^{V600E/+})/p53^{+/lf}/mitfa^{+/-} and one zebrafish with homozygous BRAF/p53 status [genotype Tg(BRAF^{V600E})/p53^{lf/lf}/mitfa^{+/-}], and GFP+ melanoma tumor cells from eight Tg(BRAF^{V600E})/p53^{lf/lf}/Tg(crestin:EGFP) fish.

Animals were euthanized using approved methods and bulk nodular tumors were excised using a razor blade. Skin samples were isolated by decapitating the euthanized zebrafish and peeling the skin off the muscle using two sets of forceps. Tumor or skin samples were manually sheared with a shortened pipette tip or using a homogenizer and then incubated in fresh 0.9× PBS with 12.5 μg/ml liberase for up to 30 min to dissociate cells. Fetal bovine serum terminated the reaction and the cells were passed through a 40 mm filter. Cells were centrifuged at 2000 × g for 5 min at 4°C. Supernatant was removed and the cells were resuspended in 500 μl 0.9× PBS and kept on ice. Fluorescence-activated cell sorting (FACS) was performed by the Washington University in St Louis core facility to isolate GFP+ tumor cells from sorted tumor samples or mCh+ melanocyte cells from sorted skin samples. Unpigmented and pigmented GFP+ and GFP- tumors were utilized to set the gating for GFP+ melanoma cells. Skin from mCh- AB* zebrafish was used to set the gating for isolating mCh+ melanocytes. Briefly, we gated first to exclude debris and doublets, then gated for the desired fluorescent marker based on comparison to a nonfluorescent sample.

Imaging

Images were acquired using a Nikon SMZ-18 with RiD2 color camera. For whole adult zebrafish images, multiple images were taken at 0.75× magnification and then merged in Adobe Lightroom 2020. Magnification of additional images for Supplementary Figure 1 specified in figure legend.

RNA library preparation and sequencing

RNA was isolated from cells using the Machery Nagel Nucleospin XS kit (Fischer Scientific cat No. NC0389511). Quantity and quality of RNA were assessed using a High Sensitivity RNA ScreenTape on an Agilent 2200 TapeStation. Sample preparation for sequencing was performed by the Genome Technology Access Center (GTAC). Briefly, cDNA was generated using a Clontech SMARTer cDNA amplification kit as per manufacturer's recommendation. 1× 50 base pair single-end sequencing was performed on an Illumina HiSeq 3000.

RNA-seq analysis

Demultiplexed fastq files were provided by the GTAC. Gene set enrichment analysis (GSEA) was performed using the GSEA software (Mootha et al. 2003; Subramanian et al. 2005). Quality of sequenced reads was assessed by FastQC (Andrews 2010). Reads were aligned to GRCz11/danRer11 by STAR with the following parameters: -outSAMtype BAM SortedByCoordinate -outFilterType BySJout -outSAMunmapped Within -outSAMattrIHstart 0 -outFilterIntronMotifs RemoveNoncanonical -quantMode TranscriptomeSAM -outSAMstrandField intronMotif (Dobin et al. 2013). Transcriptome quantification was performed by RSEM using the danRer11 NCBI RefSeq gene annotations (Li and Dewey 2011). RNA-seq reads were normalized with DESeq2 (Anders and Huber 2010). Boxplots were made using ggplot2 (Wickham 2016), heatmaps with either ggplot2 or the pheatmap function (Kolde 2015), and principal component analysis (PCA) was performed using the plotPCA function in the DESeq2 package (Anders and Huber 2010).

ATAC-seq library preparation and sequencing

Up to 50,000 cells per sample were tagged with Nextera Tn5 transposase using the Illumina Nextera kit and purified with a Qiagen MinElute reaction kit per methods modified from Buenrostro et al. (2013). The DNA was then PCR amplified to add indexing primers in nine cycles. SPRI AMPure beads enriched for fragments under ~600 bp. The library was then amplified again with the nine-cycle protocol, followed by cleanup with SPRI AMPure beads. The DNA library was quantified with a Qubit DNA High Sensitivity assay and analyzed for quality and size distribution on an Agilent 2200 TapeStation with a High Sensitivity D5000 ScreenTape. Samples were pooled at a 10 nM final concentration. Sequencing was run with an Illumina HiSeq 2500 system with 2 × 50 bp read length by the Washington University in St Louis School of Medicine GTAC.

ATAC-seq analysis

Demultiplexed fastq files were provided by GTAC. Quality of fastq files was assessed by FASTQC (Andrews 2010). Adapter sequences were removed using CutAdapt (Martin 2011), and reads were aligned to GRCz11/danRer11 using Burrows–Wheeler Aligner using default parameters (Li and Durbin 2009). BAM files were sorted using samtools, and reads with Mapping Quality (MAPQ) scores <30 and improperly paired were removed using bamtools filters with the following commands: `-mapQuality ">30" -isProperPair "true"` (Li et al. 2009; Barnett et al. 2011). We used the MarkDuplicates command from the Genome Analysis Tool Kit to remove duplicates (McKenna et al. 2010). BAM files were converted to the BED format using bedtools bamtobed command (Quinlan and Hall 2010) and used as input for peak calling with MACS2 (Zhang et al. 2008). We used the callpeak command with the following parameters: `-g 1e9, -nomodel, -extsize 100, -shift -50, -keep-dup 999, -call-summits`. Output bedGraph files were sorted, clipped, and converted to BigWig format using the bedGraphToBigWig command (Kent et al. 2010). Quality of peaks was assessed by ChIPQC (Carroll et al. 2014). The irreproducible discovery rate (IDR) was performed between replicates using the idr command (Li et al. 2011). Differentially accessible regions were called using DiffBind (Stark and Brown 2011). All motif analyses were performed using Homer (Heinz et al. 2010).

Histology

Three *Tg(mitfa:BRAF^{V600E})/p53^{lf/lf}/mitfa^{+/-}/mitfa:mCherry* zebrafish and three *Tg(mitfa:BRAF^{V600E}); p53^{lf/lf}/crestin:EGFP* zebrafish were euthanized and each whole fish was placed in a 50 ml conical with 40 ml 10% formalin for fixation and shipped to HistoWiz for further preparation. Briefly, zebrafish were decalcified and embedded; then, five sagittal sections along the midline were stained with hematoxylin and eosin.

Results

Isolating melanocyte and melanoma populations from adult zebrafish skin

To compare the transcriptional and chromatin accessibility states of normal (WT) and precancerous melanocytes (MC; harboring the BRAF^{V600E} mutation and p53^{lf} mutation) to fully transformed melanoma (MA) cells, we generated a stable transgenic zebrafish line with fluorescently labeled melanocytes expressing mCherry driven by the melanocyte-specific *melanocyte inducing transcription factor a* (*mitfa*) promoter (Ceol et al. 2011; White et al. 2011; Kaufman et al. 2016). A stable *MiniCoopR; mitfa:mCherry* transgenic line was generated in WT AB* zebrafish using Tol2-

mediated insertion (Figure 1, A and B) and then crossed to *Tg(BRAF^{V600E})/p53^{lf/lf}/mitfa^{-/-}* zebrafish (Ceol et al. 2011) to generate *Tg(BRAF^{V600E/+})/p53^{lf/lf}/mitfa^{+/-}/Tg(MiniCoopR; mitfa:mCherry)* zebrafish to investigate the impact of overactivation of BRAF in melanocytes (Figure 1, A and C and Supplementary Figure S1). Zebrafish heterozygous at the key BRAF and p53 melanoma driver loci had thicker and darker melanocyte stripes, with minor melanocyte expansion into the interstripe as compared with WT AB* fish (Figure 1, B and C and Supplementary Figure S1), consistent with the melanocyte pattern seen with homozygous BRAF^{V600E} shown previously (Patton et al. 2005). The presence of the *mitfa:mCherry* transgene did not appear to alter the normal striping pattern (whereas the presence of the BRAF and p53 alterations did, comparing Figure 1, B and C), and we detected upregulation of *mitfa* in the MA vs. both MC populations (Supplementary Table S1), consistent with prior expression studies (Kaufman et al. 2016).

Using FACS, we carefully isolated mCherry-positive (mCh+) melanocytes from *Tg(MiniCoopR; mitfa:mCherry)* (MC_WT) and *Tg(BRAF^{V600E/+})/p53^{lf/lf}/mitfa^{+/-}/Tg(MiniCoopR; mitfa:mCherry)* (MC_Het) zebrafish skin (Supplementary Figure S2, A, D, and E). We could visualize mCh+ melanocytes in both isolated scales and in the underlying hypodermis when overlying scales were removed (Supplementary Figure S2, C and D), and as we stripped the skin in its entirety after euthanasia, our melanocyte population likely includes both scale associated and hypodermal sources. mCh+ melanocyte cells were similarly ~1–5% abundant during FACS from the skin of AB* or BRAF^{V600E/+}/p53^{lf/lf}/mitfa^{+/-} zebrafish (Supplementary Figure S2). We also performed FACS on previously described Enhanced Green Fluorescent Protein (EGFP)-positive (GFP+) melanoma tumors from *Tg(BRAF^{V600E})/p53^{lf/lf}/crestin:EGFP* (MA) zebrafish to isolate melanoma cells (Figure 1D and Supplementary Figure S2, B, C, F, and H; Kaufman et al. 2016). As previously described, these melanoma tumors are identifiable as raised, highly cellular masses that are locally invasive (Supplementary Figure S2, G and H) and readily differentiated from normal skin regions, both grossly (Figure 1, B–D) and on histological sections (Supplementary Figure S2, G and H). Zebrafish *crestin* is expressed in embryonic neural crest (NC) and is re-expressed with emergence of melanoma (Kaufman et al. 2016). We then performed RNA- and ATAC-seq with each cell population (see *Materials and Methods*; Figure 1A and Supplementary Table S2).

As expected, GFP+ melanoma tumor cells and mCh+ melanocyte samples clustered based on *crestin*, EGFP, and *mCherry* normalized read counts by Euclidean distance. GFP+ samples show high *crestin* expression supporting the fidelity of the *crestin:EGFP* transgene as a faithful reporter of endogenous *crestin* expression (Figure 1E). Although melanocytes had some reads aligning to *crestin*, *crestin* expression was 109 times higher in melanoma (39,232 average reads) than in melanocytes (359 average reads), consistent with previously reported massive upregulation of *crestin* in melanoma tumors (White et al. 2011; Kaufman et al. 2016; Figure 1E).

ATAC-seq and RNA-seq libraries from sorted cells passed established Encode QC metrics for library quality and read depth. Samples for RNA-seq were sequenced to an average of 29,103,353 reads, of which 9,897,358 (34%) aligned to the transcriptome (Figure 1F). Of all genes with at least 1 count per million (CPM) mapped reads, the majority (~55%) had >10 CPM, suggesting adequate read depth. Similarly, ATAC-seq samples were sequenced to an average of 35,69,8542 paired reads of which 13,594,823 (38.1%) uniquely mapped to the genome (Figure 1G). The average fraction of uniquely mapped reads in peaks is 39.2% (Figure 1G).

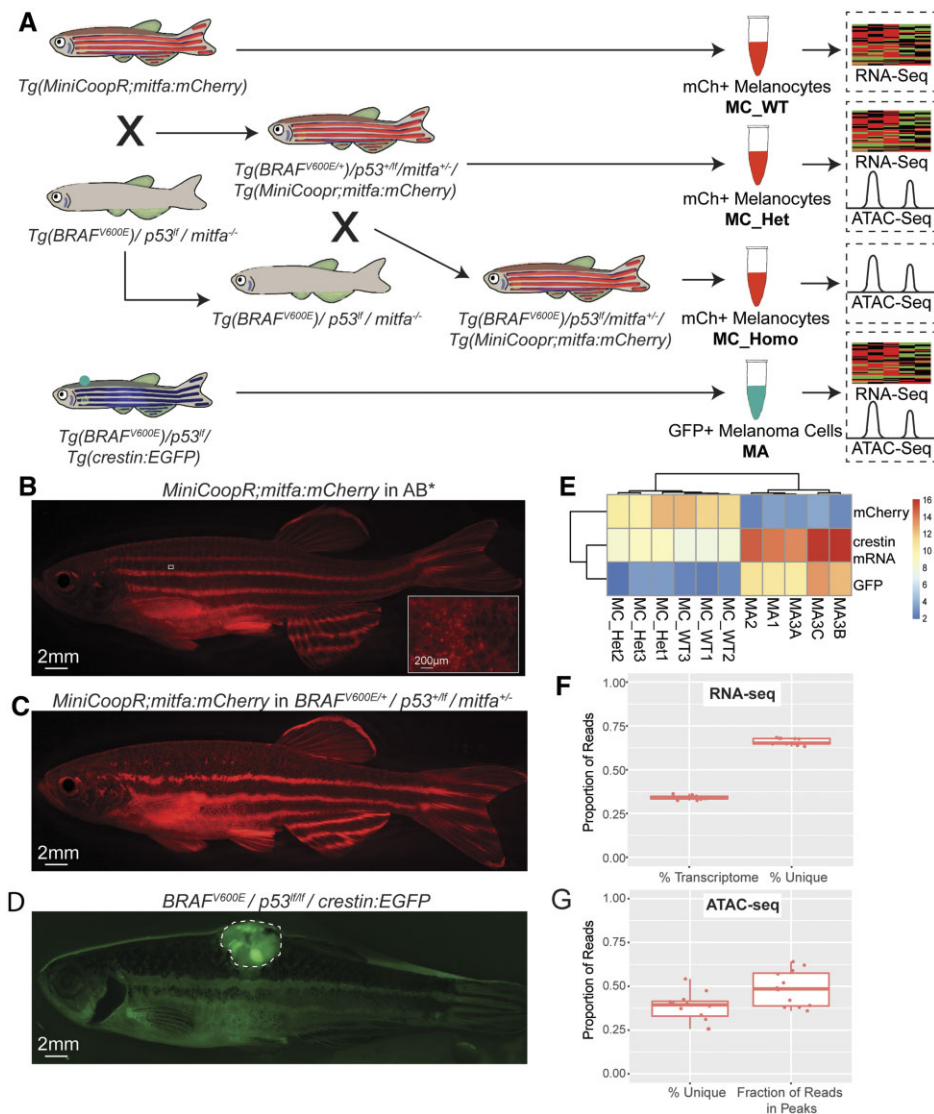


Figure 1 Isolation of zebrafish melanocytes and melanoma cells for RNA- and ATAC-seq analysis. (A) Schematic depicting experimental set up with relevant genotypes, crosses, and sources for each analysis. (B, C) Representative image of zebrafish with *mCherry* labeled melanocytes (note 7× high magnification inset with melanocytes with central dark pigment and visible surrounding fluorescence) and EGFP labeled melanoma tumor (D, outlined). (E) Heat map quantifying *mCherry*, *crestin*, and EGFP \log_2 read counts in each RNA-seq sample. (F) Quantification of proportion of unique and transcriptomic reads for RNA-seq. (G) Quantification of unique reads in ATAC-seq, and the fraction of reads located in peaks. MC, melanocyte sample; Het, heterozygous for $BRAF^{V600E}$ and *p53* transgenes; WT, wild-type AB* fish; MA, melanoma sample.

Transcriptomic comparison of normal melanocytes, BRAF/p53 mutant melanocytes, and melanoma cells

Transcriptional profiles of GFP+ (melanoma) were highly correlated (Pearson $R \geq 0.85$; Figure 2A), even from different fish. mCh+ (melanocytes) samples also had highly correlated transcriptional profiles (Figure 2A). Melanocytes from WT fish (MC_WT) and fish heterozygous for the $BRAF^{V600E}$ -driver oncogene and *p53* fl allele (MC_Het) were also highly correlated with one another with small differences in correlation coefficients between origin genotype, which is notable given the presence of the activated $BRAF^{V600E}$ oncogene in the MC_Het melanocytes ($R = 0.88$ – 0.91 within WT fish, $R = 0.85$ – 0.87 within heterozygotes, and $R = 0.85$ – 0.87 across genotypes; Figure 2A). Melanoma samples were similarly highly correlated ($R = 0.87$ – 0.93) with slightly higher correlation for multiple tumors isolated from the same fish ($R = 0.93$ for MA3A, MA3B, MA3C, and $R = 0.87$ – 0.92 for

external replicates). Melanocytes and melanoma cells readily separated using unsupervised hierarchical clustering (correlation coefficients between 0.74 and 0.81) indicating that transcriptional profiles alter during transformation from a BRAF mutant melanocyte to a fully oncogenic melanoma cell, but remain more closely correlated in a WT (MC_WT) or premalignant (MC_Het) state. Furthermore, PCA readily separates melanocytes from melanomas, with the first principal component accounting for 38% of the variance (Figure 2B). Principal component two (accounting for 11% of the variance) likely captures the lesser transcriptional differences between the WT and Het MC samples.

We identified 1144 genes significantly upregulated in melanomas vs. melanocytes, and 2984 genes significantly upregulated in melanocytes compared with melanoma cells [\log_2 fold change (\log_2FC) > 1 and adjusted P -value $< 10^{-6}$, Supplementary Figure S3A]. Surprisingly, the number of melanoma-upregulated genes meeting increasing log fold change cutoffs dropped off more

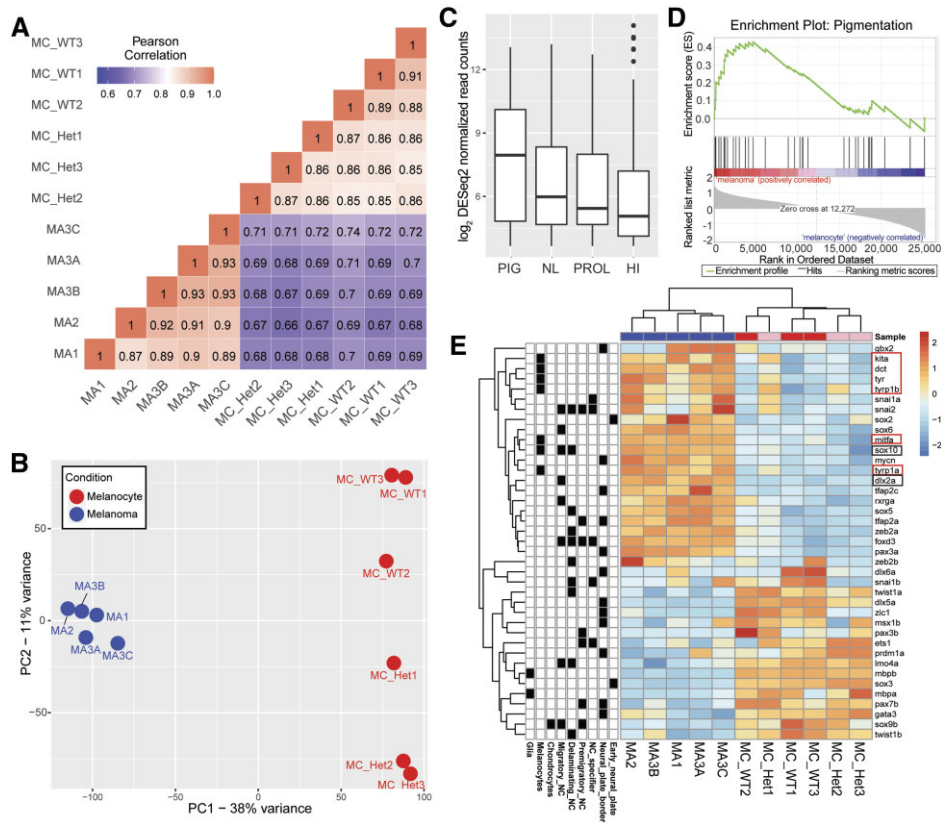


Figure 2 RNA-seq analysis of melanocyte and melanoma cell populations. (A) Correlation plot depicting the Pearson correlation between each sample. (B) PCA plot with the components with the highest variation. (C) Box plot comparing zebrafish ortholog expression in melanoma cells of genes associated with 4 subtypes of human melanoma (Jönsson et al. 2010). PIG, pigmentation (median = 7.950548); NL, normal-like (median = 5.982954); PROL, proliferative (median = 5.43669); HI, high immune (median = 5.063983). (D) Positive correlation using GSEA of genes associated with the pigmentation subtype of human melanoma and zebrafish upregulated melanoma genes. Enrichment score = 0.4299, P -value = 0.036, q -value = 0.134. (E) Heat map depicting relative gene expression between zebrafish melanoma and melanocyte populations for NC genes associated with specific NC populations (e.g., early NC, neural plate border) or descendant lineages (e.g., glia, chondrocytes, melanocytes). NC genes of note in black boxes. Select melanocyte genes in red boxes. MC, melanocyte sample; Het, heterozygous for $BRAF^{V600E}$ and $p53$ transgenes; WT, wild-type AB^+ fish; MA, melanoma sample.

steeply than melanocyte-upregulated genes, indicating that more genes are downregulated in melanoma as compared with melanocytes (Supplementary Figure S3B).

Comparing WT and Het ($Tg(BRAF^{V600E/+})/p53^{+/-}$) melanocytes, there are far fewer significantly differentially expressed genes with 12 genes upregulated in WT over Het melanocytes and 41 genes upregulated in Het over WT melanocytes with $\log_2FC > 1$ and adjusted P -value $\leq 10^{-6}$ (Supplementary Figure S3C). These results highlight the surprising similarity within melanocytes and premalignant (i.e., $BRAF$ mutant/ $p53$ mutant) melanocytes as compared with the more dramatic changes that occur when compared with transformed melanocytes/melanoma. To facilitate further inquiry, we provide a list of all gene expression changes and P -values between melanocytes, premalignant melanocytes, and melanoma cells (Supplementary Table S1).

Gene expression programs

We compared gene expression profiles between our melanocyte and melanoma samples to the four gene lists from Jönsson et al. (2010) stratifying human cutaneous melanoma into proliferative, pigmentation, high immune, and normal-like subtypes. First, we assessed which subtype of human melanoma our zebrafish melanoma samples most resembled and

found the highest average expression of genes associated with the pigmentation subtype (Figure 2C). This was further confirmed with GSEA detecting significant enrichment of genes associated with the human melanoma pigmentation subtype (GSEA ES = 0.4299, $P = 0.036$; Figure 2D). Finally, comparing expression in zebrafish melanocytes to melanoma cells, genes in the pigmentation list had the most significant upregulation in melanoma cells (paired P -value = 0.007; Supplementary Figure S3, D–H).

Previous studies have shown that melanoma reactivates aspects of an embryonic NC program, with prominent NC genes such as *sox10* the subject of much interest (Shakhova et al. 2012; Cronin et al. 2013; Mohamed et al. 2013; Kaufman et al. 2016). The central gene regulatory network, or “wiring diagram,” for NC development has been well-described, and we used the NC gene regulatory network described by Kunz et al. (2018) to examine gene expression changes in each condition for NC pathway genes (Supplementary Table S3). We found *sox10* and *dlx2a* are upregulated in melanoma in agreement with previous smaller scale transcriptional analyses (black boxes, Figure 2E; Kaufman et al. 2016). Interestingly, important melanocyte-specific genes including *mitfa*, *tyrp1b*, *kita*, *dct*, *tyr*, and *tyrp1a* were upregulated in the melanoma samples, supporting that melanoma cells sustain a

continued presence of an active melanocyte identity (red boxes, Figure 2E). To further probe this finding, we assessed whether either cell population had enrichment of human melanocyte genes (Reemann et al. 2014). Indeed, both zebrafish melanocytes and melanoma cells had high expression of human melanocyte genes (Supplementary Figure S3H).

Another recurring and important question relates to the idea that the NC incorporates a spectrum of developmental time (e.g., from specification, to delamination, to migration, etc.), spatial differences (e.g., cranial, thoracic, caudal NC), and descendant lineages (e.g., glia, melanocyte, chondrocyte), each with defining genetic markers in its transcriptional program (Supplementary Table S3; Simões-Costa and Bronner 2015; Williams et al. 2019). We reviewed our melanoma differential gene sets in relation to these NC subsets and, aside from a “strengthening” of the melanocyte program as noted above and decrease in expression of glial (*mbpa/b*) and chondrocyte (*sox9b*) factors, we did not note other clear unifying NC subsets that aligned more closely to the melanoma program (Figure 2E). Given the widespread dysregulation of gene expression in the cancerous melanoma state, this is perhaps unsurprising that the malignant phenotype would entail a broad and not entirely faithful amalgamation of melanocyte and NC transcriptional identities.

Chromatin accessibility profiles in melanocytes and melanoma cells

To characterize the genome-wide chromatin accessibility of pre-malignant *Tg(BRAF^{V600E})/p53^{lfl/fl}* mutant melanocytes and melanoma, we isolated pre-malignant melanocytes (mCh+) from four zebrafish, including three MC_Het and one sample from a *Tg(BRAF^{V600E})/p53^{lfl/fl}/Tg(MiniCoopR; mitfa:mCherry)* zebrafish (MC_Homo). Since MC_WT and MC_Het read counts were highly correlated in the RNA-seq, we utilized MC_Het zebrafish for ATAC-seq analysis. We compared these profiles to those from eight melanoma tumors sorted for *crestin:EGFP* expression (Figure 3A).

As in the RNA-seq analysis, melanocyte samples and melanoma samples clustered according to normal vs. malignant state (Figure 3, A and B). To assess the reproducibility of each identified accessible site within a condition, we evaluated the IDR, setting a threshold of 0.05. For MC samples, an average of 53% of sites passed IDR 0.05, and for the MA samples, the average was 33% (Supplementary Figure S4A).

In our ATAC-Seq analysis, 56,936 sites demonstrated differential accessibility ($P < 0.05$, $IDR < 0.05$) between melanocyte and melanoma cells. Open regions, or peaks, within 3 kilobases (kb) of transcriptional start sites (TSS) were centered at the TSS

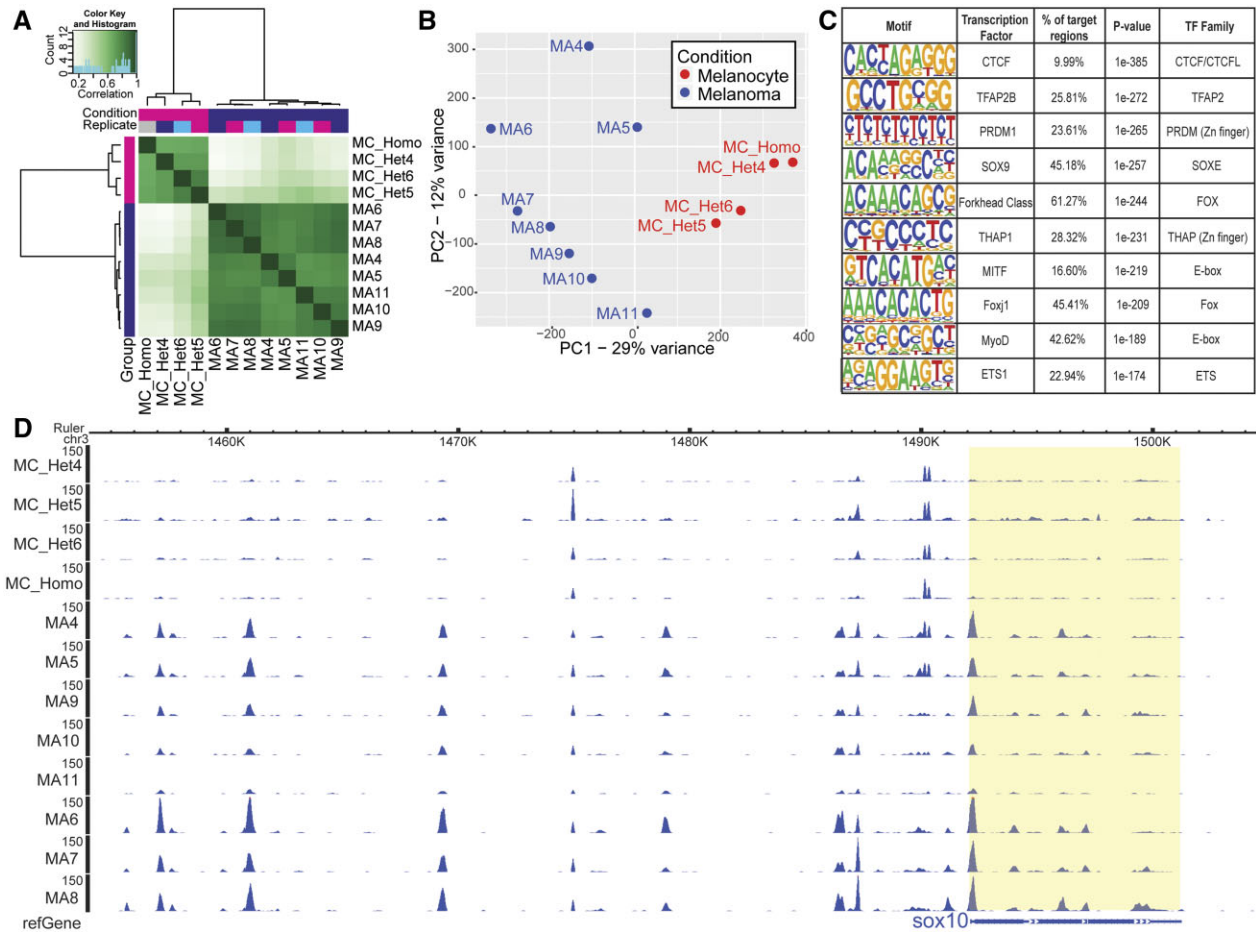


Figure 3 ATAC-seq analysis of melanocyte and melanoma cells. (A) Correlation plot of overall chromatin accessibility across the genome, with darker green color indicating greater correlation between samples. (B) PCA plot comparing similarity of chromatin accessibility across conditions. (C) Predicted TF binding sites, based on HOMER analysis, enriched in open chromatin domains more accessible in melanoma vs. melanoma cells. Each TF is reported with its associated TF family, as TF families frequently have similar or identical binding sites which are not differentiated by HOMER. (D) Epigenome browser tracks near and upstream of the NC and melanoma gene *sox10* on chromosome 3. MC, melanocyte sample; Het, heterozygous for *BRAF^{V600E}* and *p53* transgenes; Homo, homozygous for *BRAF^{V600E}* and *p53* transgenes; MA, melanoma sample.

(Supplementary Figure S4B). Of promoter annotated peaks, 85% of differentially accessible sites were more open in melanoma as compared with melanocytes (Supplementary Figure S4C and Table S4).

Open chromatin regions and putative transcription factor binding sites

We examined the differentially accessible chromatin regions using HOMER *de novo* analysis to identify over-represented DNA motifs representing putative transcription factor (TF) binding sites (Figure 3D). In order of significance, sites associated with CCCTC-binding factor (CTCF) topped the list—a TF commonly mutated in cancer and known to normally function widely in controlling chromatin architecture (Kim et al. 2015). TF binding motif families corresponding to key NC-associated factors also rounded out the top 10 list, including the Forkhead, SOXE, and ETS families. Melanocyte and NC programs are particularly active in melanoma cells, with increased *sox10* and *mitfa* expression, respectively, seen in the RNA-seq data (Figure 2E), and this appears consistent with enrichment of SOX9/10 (SOXE family)

and MITF (E/M-boxes) binding sites in more accessible regions in melanoma (Figure 3C). Finally, we noted the overall similarity in the contour of chromatin accessibility within premalignant melanocytes and melanomas as well as the numerous areas of differential accessibility as, for example, near *sox10* and *mitfa* (Figure 3D and Supplementary Figure S4D).

Modeling gene expression as a function of peak accessibility

To examine potential relationships between open chromatin and gene expression, we assessed the relationship between \log_2FC for differentially expressed genes and differentially accessible promoter peaks. As expected, the majority of genes with greater expression in melanoma had more accessibility with peaks within 3 kb of the promoter ($n = 2386$ pairs of genes and peaks; one gene can be linked to multiple ATAC-seq peaks), while genes with less expression were less accessible at the promoter ($n = 499$). Interestingly, 1213 genes had greater accessibility at the promoter in melanoma, yet had lower expression. We then focused on evaluating the relationship between accessibility and

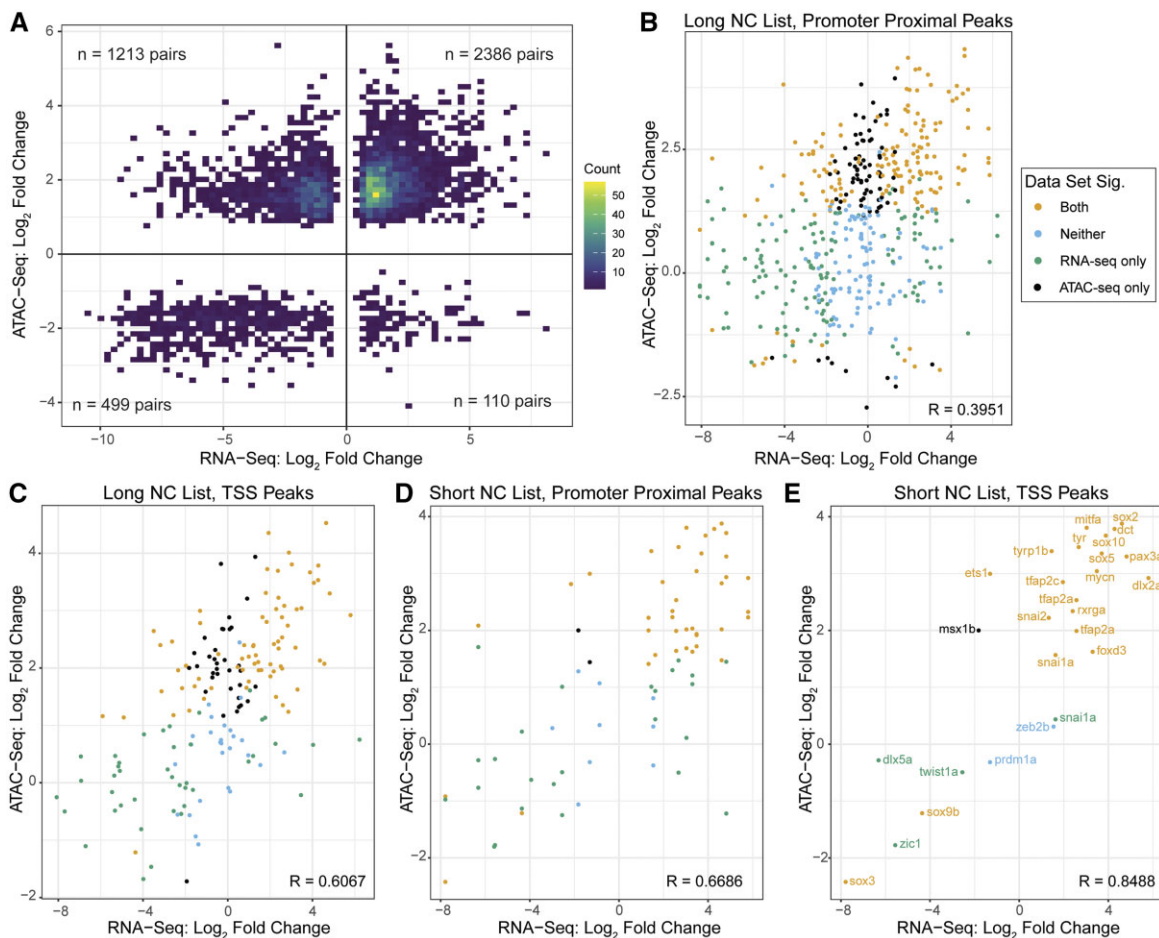


Figure 4. Integration of gene expression and accessibility. (A) Significantly differentially expressed genes between melanoma and melanocyte cells (RNA-seq, $|\log_2FC| > 1$, $P < 0.05$) plotted against the most differentially accessible peak (ATAC-Seq, $|\log_2FC| > 1$, $P < 0.05$) within 3 kb of each gene's promoter. Genes upregulated in melanoma are to the right, and genes with a more open chromatin region near the promoter in melanoma are on the top half. (B, C) All genes from ZFIN.org associated with NC (long list, Supplementary Table S3) with expression plotted with all accessible peaks (B) within 3 kb of the TSS (Pearson correlation coefficient $R = 0.3951$) and (C) only at the TSS ($R = 0.6067$). Points representing genes significantly differentially expressed ($|\log_2FC| > 1$, $P < 0.05$) in RNA-seq are in green, points representing peaks significantly differentially accessible in ATAC-seq ($|\log_2FC| > 1$, $P < 0.05$) are in black, points neither significantly expressed nor significantly accessible in blue, and points representing genes and peaks which are both significantly differentially expressed and significantly differentially accessible are in pink. (D, E) Genes associated with specific NC gene regulatory network stages discussed in the literature (shortlist, Supplementary Table S3) with expression plotted with all peaks (D) within 3 kb of the TSS ($R = 0.6686$) and (E) at the TSS with each point labeled with the gene name ($R = 0.8488$). Significance color scheme same as in (B, C).

expression in NC genes using a “long list” of 329 genes associated with NC from ZFIN.org and a curated shortlist of 44 genes associated with specific NC developmental stages (Supplementary Tables S3 and S5). Utilizing the long list, we found a modest correlation (Pearson’s correlation coefficient $R=0.3951$) between gene expression accessibility at promoter-proximal peaks within 3 kb of the promoter (Figure 4B). This relationship was strengthened when focusing only on peaks at the TSS (Figure 4C; $R=0.6067$). Further, focusing specifically on genes previously shown to be involved in NC development, this association was even more pronounced (Figure 4D; $R=0.6686$), with peaks at the promoter showing a clear correlation with expression (Figure 4E; $R=0.8488$).

Discussion

Here, we present a zebrafish model allowing for efficient isolation of melanocytes and melanoma cells and provide a resource capturing transcriptional and chromatin accessibility changes occurring *in vivo* during *de novo* tumor development. Independent replicates from genetically related animals add robustness to the dataset while limiting the background genetic complexity of a fully outbred population. This combined RNA- and ATAC-seq analysis of normal, premalignant, and transformed melanocytes/melanoma offers a tool for gene and pathway discovery in melanoma biology. Moreover, the tumor diversity with pigmentation status and tumor location (Supplementary Table S2) provides a comprehensive picture of cutaneous melanoma in a BRAF-driven, MITF-high model (Travnickova et al. 2019). Based on widely used QC metrics, we conclude that our RNA- and ATAC-seq data accurately reflect the *in vivo* transcriptional and chromatin accessibility state of the average premalignant BRAF/p53 mutant melanocyte and melanoma cell and provide an important and broadly useful tool for further investigating transcriptional and epigenetic programs underlying these related but crucially different pre- and fully malignant states. Similar studies have shed light on the epigenetic regulation of dysregulated genes that promote melanoma, such as *sox10* (Cunningham et al. 2021), or have been used to delineate developmental programs underlying erythroid differentiation (Ludwig et al. 2019). Studies have found a reactivation of an NC program in melanoma (Kaufman et al. 2016), and indeed we observed upregulation of NC genes such as *crestin*, *sox10*, *tfap2a*, *dlx2a*, among others. However, when we expanded the analysis to include NC genes segregated by stage of expression in NC, there was not a clear program upregulated in melanoma (*i.e.*, not all migratory NC markers were upregulated). This further supports a widespread dysregulation of expression programs in the disease state and begs the question of which consistent gene program is reactivated in melanoma. Nevertheless, there is an apparent relationship between accessibility at the TSS and gene expression of NC-associated genes (Figure 4E).

Interestingly, our dataset shows that in melanoma there are more genes with significant downregulation in melanoma relative to melanocytes, despite the presence of more accessible regions in the melanoma genome, supporting previous findings that points of control other than promoter accessibility, such as TF and chromatin regulatory protein abundances and activities, may be primary influencers of gene expression and thus changes in cell identity in the transition to a malignant state (Travnickova et al. 2019; Santoriello et al. 2020; Baggiolini et al. 2021; Fazio et al. 2021; Terranova et al. 2021). Indeed, it has been shown that very distal enhancers can control gene expression, indicating that

open regions of chromatin may not necessarily regulate the most proximal gene (Lettice et al. 2003; Amano et al. 2009; Lacomme et al. 2018). Most changes in accessibility occur in distal nonpromoter regions (Supplementary Figure S4C; Thurman et al. 2012; Pliner et al. 2018; Friman et al. 2019), and deciphering the relationship between gene expression and cis-regulatory regions has been a topic of immense focus (Ackermann et al. 2016; Gonen et al. 2018; Zhao et al. 2019; Cai et al. 2020; Cunningham et al. 2021; Panigrahi and O’Malley 2021). Our study serves as a foundation to probe open chromatin regions and potential regulatory functions.

Furthermore, though all samples had an active melanocyte-specific program, genes typically associated with melanocytes were upregulated and more accessible in melanoma, consistent with a widespread dysregulation in additional gene programs in the melanoma cell state. We anticipate these data will contribute to ongoing functional analyses testing candidates that control the crucial epigenetic and transcriptional differences driving the transition between the normal and diseased cell state.

Data availability

Strains are available upon request. BigWig files can be found on the Gene Expression Omnibus, accession no. GSE178803. Supplementary files submitted through figshare (<https://doi.org/10.25387/g3.16841419>).

Acknowledgments

We thank the Genome Technology Access Center in the Department of Genetics at Washington University School of Medicine for help with genomic analysis. The Center is partially supported by NCI Cancer Center Support Grant No. P30 CA91842 to the Siteman Cancer Center and by ICTS/CTSA Grant No. UL1 TR000448 from the National Center for Research Resources (NCRR), a component of the National Institutes of Health (NIH), and NIH Roadmap for Medical Research. This publication is solely the responsibility of the authors and does not necessarily represent the official view of NCRR or NIH. We also thank the Fluorescence-Activated Cell Sorting core for their assistance with sorting our samples.

Funding

Research reported in this publication was supported in part by the National Cancer Institute of the National Institutes of Health under award number R01CA240633. The content is solely the responsibility of the authors and does not necessarily represent the official views of the National Institutes of Health. C.K.K. was funded by the Cancer Research Foundation Young Investigator Award and R01CA240633. E.T.K. was supported by the National Institutes of Health Kirschstein National Research Service Award Institutional Research Training Grant T32# GM007067 during data collection. P.M.G. was supported by the National Science Foundation Graduate Research Fellowship (DEG-1745038).

Conflict of interest

The authors declare no conflict of interest.

Literature cited

- Ackermann AM, Wang Z, Schug J, Naji A, Kaestner KH. 2016. Integration of ATAC-seq and RNA-seq identifies human alpha cell and beta cell signature genes. *Mol Metab.* 5:233–244.
- Amano T, Sagai T, Tanabe H, Mizushima Y, Nakazawa H, et al. 2009. Chromosomal dynamics at the *Shh* locus: limb bud-specific differential regulation of competence and active transcription. *Dev Cell.* 16:47–57.
- Anders S, Huber W. 2010. Differential expression analysis for sequence count data. *Genome Biol.* 11:R106.
- Andrews S. 2010. FASTQC: a quality control tool for high throughput sequence data. <http://www.Bioinformatics.Babraham.Ac.Uk/projects/fastqc> (Accessed: 2021 November 10).
- Badal B, Solovyov A, Di Cecilia S, Chan JM, Chang L-W, et al. 2017. Transcriptional dissection of melanoma identifies a high-risk subtype underlying TP53 family genes and epigenome deregulation. *JCI Insight.* 2:e92102.
- Baggiolini A, Callahan S. J., Montal, E, Weiss, J. M., Trieu, T, et al. 2021. Developmental chromatin programs determine oncogenic competence in melanoma. *Science.* 373:eabc1048.
- Barnett DW, Garrison EK, Quinlan AR, Stromberg MP, Marth GT. 2011. Bamtools. *Bioinformatics.* 27:1691–1692.
- Baron M, Tagore M, Hunter MV, Kim IS, Moncada R, et al. 2020. The stress-like cancer cell state is a consistent component of tumorigenesis. *Cell Syst.* 11:536–546.e7.
- Belote RL, Le D, Maynard A, Lang UE, Sinclair A, et al. 2021. Human melanocyte development and melanoma dedifferentiation at single-cell resolution. *Nat Cell Biol.* 23:1035–1047.
- Buenrostro JD, Giresi PG, Zaba LC, Chang HY, Greenleaf WJ. 2013. Transposition of native chromatin for fast and sensitive epigenomic profiling of open chromatin, DNA-binding proteins and nucleosome position. *Nat Methods.* 10:1213–1218.
- Cai W, Huang J, Zhu Q, Li BE, Seruggia D, et al. 2020. Enhancer dependence of cell-type-specific gene expression increases with developmental age. *Proc Natl Acad Sci U S A.* 117:21450–21458.
- Cancer Genome Atlas Network. 2015. Genomic classification of cutaneous melanoma. *Cell.* 161:1681–1696.
- Carroll TS, Liang Z, Salama R, Stark R, de Santiago I. 2014. Impact of artifact removal on ChIP quality metrics in ChIP-seq and ChIP-exo data. *Front Genet.* 5:75–75.
- Ceol CJ, Houvras Y, Jane-Valbuena J, Bilodeau S, Orlando DA, et al. 2011. The histone methyltransferase SETDB1 is recurrently amplified in melanoma and accelerates its onset. *Nature.* 471:513–517.
- Cirenajwis H, Ekedahl H, Lauss M, Harbst K, Carneiro A, et al. 2015. Molecular stratification of metastatic melanoma using gene expression profiling: prediction of survival outcome and benefit from molecular targeted therapy. *Oncotarget.* 6:12297–12309.
- Cisarova K, Folcher M, El Zaoui I, Pescini-Gobert R, Peter VG, et al. 2020. Genomic and transcriptomic landscape of conjunctival melanoma. *PLoS Genet.* 16:e1009201.
- Corces MR, Buenrostro JD, Wu B, Greenside PG, Chan SM, et al. 2016. Lineage-specific and single-cell chromatin accessibility charts human hematopoiesis and leukemia evolution. *Nat Genet.* 48:1193–1203.
- Cronin JC, Watkins-Chow DE, Incao A, Hasskamp JH, Schönewolf N, et al. 2013. SOX10 ablation arrests cell cycle, induces senescence, and suppresses melanomagenesis. *Cancer Res.* 73:5709–5718.
- Cunningham RL, Kramer ET, DeGeorgia SK, Godoy PM, Zarov AP, et al. 2021. Functional *in vivo* characterization of *sox10* enhancers in neural crest and melanoma development. *Commun Biol.* 4:695.
- Dobin A, Davis CA, Schlesinger F, Drenkow J, Zaleski C, et al. 2013. Star: ultrafast universal RNA-seq aligner. *Bioinformatics.* 29:15–21.
- Durante MA, Rodriguez DA, Kurtenbach S, Kuznetsov JN, Sanchez MI, et al. 2020. Single-cell analysis reveals new evolutionary complexity in uveal melanoma. *Nat Commun.* 11:496.
- Ennen M, Keime C, Kobi D, Mengus G, Lipsker D, et al. 2015. Single-cell gene expression signatures reveal melanoma cell heterogeneity. *Oncogene.* 34:3251–3263.
- Fazio M, van Rooijen E, Dang M, van de Hoek G, Ablain J, et al. 2021. SATB2 induction of a neural crest mesenchyme-like program drives melanoma invasion and drug resistance. *Elife.* 10:e64370.
- Friman ET, Deluz C, Meireles-Filho ACA, Govindan S, Gardeux V, et al. 2019. Dynamic regulation of chromatin accessibility by pluripotency transcription factors across the cell cycle. *Elife.* 8:e50087.
- Gan Y, Li N, Zou G, Xin Y, Guan J. 2018. Identification of cancer subtypes from single-cell RNA-seq data using a consensus clustering method. *BMC Med Genomics.* 11:117.
- Garg M, Couturier D-L, Nsengimana J, Fonseca NA, Wongchenko M, et al. 2021. Tumour gene expression signature in primary melanoma predicts long-term outcomes. *Nat Commun.* 12:1137.
- Gonen N, Futtner CR, Wood S, Garcia-Moreno SA, Salamone IM, et al. 2018. Sex reversal following deletion of a single distal enhancer of *Sox9*. *Science.* 360:1469–1473.
- Haltaufderhyde KD, Oancea E. 2014. Genome-wide transcriptome analysis of human epidermal melanocytes. *Genomics.* 104:482–489.
- Harbst K, Staaf J, Lauss M, Karlsson A, Måsbäck A, et al. 2012. Molecular profiling reveals low- and high-grade forms of primary melanoma. *Clin Cancer Res.* 18:4026–4036.
- Hayward NK, Wilmott JS, Waddell N, Johansson PA, Field MA, et al. 2017. Whole-genome landscapes of major melanoma subtypes. *Nature.* 545:175–180.
- Heinz S, Benner C, Spann N, Bertolino E, Lin YC, et al. 2010. Simple combinations of lineage-determining transcription factors prime cis-regulatory elements required for macrophage and B cell identities. *Mol Cell.* 38:576–589.
- Hodis E, Watson IR, Kryukov GV, Arold ST, Imielinski M, et al. 2012. A landscape of driver mutations in melanoma. *Cell.* 150:251–263.
- Jönsson G, Busch C, Knappskog S, Geisler J, Miletic H, et al. 2010. Gene expression profiling-based identification of molecular subtypes in stage IV melanomas with different clinical outcome. *Clin Cancer Res.* 16:3356–3367.
- Kaufman CK, Mosimann C, Fan ZP, Yang S, Thomas AJ, et al. 2016. A zebrafish melanoma model reveals emergence of neural crest identity during melanoma initiation. *Science.* 351:aad2197.
- Kent WJ, Zweig AS, Barber G, Hinrichs AS, Karolchik D. 2010. Bigwig and bigbed: enabling browsing of large distributed datasets. *Bioinformatics.* 26:2204–2207.
- Kim S, Yu N-K, Kaang B-K. 2015. CTCF as a multifunctional protein in genome regulation and gene expression. *Exp Mol Med.* 47:e166.
- Kolde R. 2015. Pheatmap: pretty heatmaps [software]. <https://CRAN.R-project.org/package=pheatmap> (Accessed: 2021 November 10).
- Kunz M, Löffler-Wirth H, Dannemann M, Willscher E, Doose G, et al. 2018. RNA-seq analysis identifies different transcriptomic types and developmental trajectories of primary melanomas. *Oncogene.* 37:6136–6151.
- Lacomme M, Medevielle F, Bourbon H-M, Thierion E, Kleinjan D-J, et al. 2018. A long range distal enhancer controls temporal fine-tuning of PAX6 expression in neuronal precursors. *Dev Biol.* 436:94–107.

- Lauss M, Nsengimana J, Staaf J, Newton-Bishop J, Jönsson G. 2016. Consensus of melanoma gene expression subtypes converges on biological entities. *J Invest Dermatol.* 136:2502–2505.
- Lettice LA, Heaney SJ, Purdie LA, Li L, de Beer P, et al. 2003. A long-range Shh enhancer regulates expression in the developing limb and fin and is associated with preaxial polydactyly. *Hum Mol Genet.* 12:1725–1735.
- Li B, Dewey CN. 2011. RSEM: accurate transcript quantification from RNA-seq data with or without a reference genome. *BMC Bioinformatics.* 12:323.
- Li H, Durbin R. 2009. Fast and accurate short read alignment with burrows-wheeler transform. *Bioinformatics.* 25:1754–1760.
- Li H, Handsaker B, Wysoker A, Fennell T, Ruan J, et al.; 1000 Genome Project Data Processing Subgroup. 2009. The sequence alignment/map format and samtools. *Bioinformatics.* 25:2078–2079.
- Li Q, Brown JB, Huang H, Bickel PJ. 2011. Measuring reproducibility of high-throughput experiments. *Ann Appl Stat.* 5:1752–1779.
- Li X, Karras P, Torres R, Rambow F, van den Oord J, et al. 2020. Disseminated melanoma cells transdifferentiate into endothelial cells in intravascular niches at metastatic sites. *Cell Rep.* 31:107765.
- Ludwig LS, Lareau CA, Bao EL, Nandakumar SK, Muus C, et al. 2019. Transcriptional states and chromatin accessibility underlying human erythropoiesis. *Cell Rep.* 27:3228–3240.e7.
- Marie KL, Sassano A, Yang HH, Michalowski AM, Michael HT, et al. 2020. Melanoblast transcriptome analysis reveals pathways promoting melanoma metastasis. *Nat Commun.* 11:333.
- Martin M. 2011. Cutadapt removes adapter sequences from high-throughput sequencing reads. *EMBnet J.* 17:10–12.
- McKenna A, Hanna M, Banks E, Sivachenko A, Cibulskis K, et al. 2010. The genome analysis toolkit: a mapreduce framework for analyzing next-generation DNA sequencing data. *Genome Res.* 20:1297–1303.
- Mohamed A, Gonzalez RS, Lawson D, Wang J, Cohen C. 2013. SOX10 expression in malignant melanoma, carcinoma, and normal tissues. *Appl Immunohistochem Mol Morphol.* 21:506–510.
- Mootha VK, Lindgren CM, Eriksson K-F, Subramanian A, Sihag S, et al. 2003. PGC-1 α -responsive genes involved in oxidative phosphorylation are coordinately downregulated in human diabetes. *Nat Genet.* 34:267–273.
- Nsengimana J, Laye J, Filia A, Walker C, Jewell R, et al. 2015. Independent replication of a melanoma subtype gene signature and evaluation of its prognostic value and biological correlates in a population cohort. *Oncotarget.* 6:11683–11693.
- Panigrahi A, O'Malley BW. 2021. Mechanisms of enhancer action: the known and the unknown. *Genome Biol.* 22:108.
- Patton EE, Widlund HR, Kutok JL, Kopani KR, Amatruda JF, et al. 2005. BRAF mutations are sufficient to promote nevi formation and cooperate with p53 in the genesis of melanoma. *Curr Biol.* 15:249–254.
- Pliner HA, Packer JS, McFaline-Figueroa JL, Cusanovich DA, Daza RM, et al. 2018. Cicero predicts cis-regulatory DNA interactions from single-cell chromatin accessibility data. *Mol Cell.* 71:858–871.e8.
- Quinlan AR, Hall IM. 2010. Bedtools: a flexible suite of utilities for comparing genomic features. *Bioinformatics.* 26:841–842.
- Rabbie R, Ferguson P, Molina-Aguilar C, Adams DJ, Robles-Espinoza CD. 2019. Melanoma subtypes: genomic profiles, prognostic molecular markers and therapeutic possibilities. *J Pathol.* 247:539–551.
- Rambow F, Rogiers A, Marin-Bejar O, Aibar S, Femel J, et al. 2018. Toward minimal residual disease-directed therapy in melanoma. *Cell.* 174:843–855.e19.
- Reemann P, Reimann E, Ilmjärv S, Porosaar O, Silm H, et al. 2014. Melanocytes in the skin—comparative whole transcriptome analysis of main skin cell types. *PLoS One.* 9:e115717.
- Reuben A, Spencer CN, Prieto PA, Gopalakrishnan V, Reddy SM, et al. 2017. Genomic and immune heterogeneity are associated with differential responses to therapy in melanoma. *NPJ Genomic Med.* 2:10.
- Sakabe NJ, Aneas I, Knoblauch N, Sobreira DR, Clark N, et al. 2020. Transcriptome and regulatory maps of decidua-derived stromal cells inform gene discovery in preterm birth. *Sci Adv.* 6:eabc8696.
- Santoriello C, Sporrij A, Yang S, Flynn RA, Henriques T, et al. 2020. RNA helicase ddx21 mediates nucleotide stress responses in neural crest and melanoma cells. *Nat Cell Biol.* 22:372–379.
- Shakhova O, Zingg D, Schaefer SM, Hari L, Civenni G, et al. 2012. Sox10 promotes the formation and maintenance of giant congenital naevi and melanoma. *Nat Cell Biol.* 14:882–890.
- Simões-Costa M, Bronner ME. 2015. Establishing neural crest identity: a gene regulatory recipe. *Development.* 142:242–257.
- Stark R, Brown G. 2011. DiffBind: differential binding analysis of ChIP-seq peak data. <https://bioconductor.org/packages/release/bioc/html/DiffBind.html>. (Accessed: 2021 November 10).
- Subramanian A, Tamayo P, Mootha VK, Mukherjee S, Ebert BL, et al. 2005. Gene set enrichment analysis: a knowledge-based approach for interpreting genome-wide expression profiles. *Proc Natl Acad Sci USA.* 102:15545–15550.
- Terranova CJ, Tang M, Maitiuheti M, Raman AT, Ghosh AK, et al. 2021. Reprogramming of bivalent chromatin states in NRAS mutant melanoma suggests PRC2 inhibition as a therapeutic strategy. *Cell Rep.* 36:109410.
- Thurman RE, Rynes E, Humbert R, Vierstra J, Maurano MT, et al. 2012. The accessible chromatin landscape of the human genome. *Nature.* 489:75–82.
- Tirosh I, Venteicher AS, Hebert C, Escalante LE, Patel AP, et al. 2016. Single-cell RNA-seq supports a developmental hierarchy in human oligodendrogloma. *Nature.* 539:309–313.
- Travnickova J, Patton EE. 2021. Deciphering melanoma cell states and plasticity with zebrafish models. *J Invest Dermatol.* 141:1389–1394.
- Travnickova J, Wojciechowska S, Khamseh A, Gautier P, Brown DV, et al. 2019. Zebrafish MITF-low melanoma subtype models reveal transcriptional subclusters and MITF-independent residual disease. *Cancer Res.* 79:5769–5784.
- Tsoi J, Robert L, Paraiso K, Galvan C, Sheu KM, et al. 2018. Multi-stage differentiation defines melanoma subtypes with differential vulnerability to drug-induced iron-dependent oxidative stress. *Cancer Cell.* 33:890–904.e5.
- Venkatesan AM, Vyas R, Gramann AK, Dresser K, Gujja S, et al. 2018. Ligand-activated BMP signaling inhibits cell differentiation and death to promote melanoma. *J Clin Invest.* 128:294–308.
- White RM, Cech J, Ratanasirintrao S, Lin CY, Rahl PB, et al. 2011. DHODH modulates transcriptional elongation in the neural crest and melanoma. *Nature.* 471:518–522.
- Wickham H. 2016. Ggplot2: Elegant Graphics for Data Analysis. New York, NY: Springer-Verlag.
- Williams RM, Candido-Ferreira I, Repapi E, Gavriouchkina D, Senanayake U, et al. 2019. Reconstruction of the global neural crest gene regulatory network in vivo. *Dev Cell.* 51:255–276.e7.
- Wouters J, Kalender-Atak Z, Minnoye L, Spanier KI, De Waegeneer M, et al. 2020. Robust gene expression programs underlie recurrent cell states and phenotype switching in melanoma. *Nat Cell Biol.* 22:986–998.

Yen J, White RM, Wedge DC, Van Loo P, de Ridder J, et al. 2013. The genetic heterogeneity and mutational burden of engineered melanomas in zebrafish models. *Genome Biol.* 14: R113.

Zhang Y, Liu T, Meyer CA, Eeckhoutte J, Johnson DS, et al. 2008. Model-based analysis of ChIP-seq (macs). *Genome Biol.* 9: R137.

Zhao Y, Zheng D, Cvekl A. 2019. Profiling of chromatin accessibility and identification of general cis-regulatory mechanisms that control two ocular lens differentiation pathways. *Epigenetics Chromatin.* 12:27.

Communicating editor: B. Andrews